Available online at www.sciencedirect.com

ScienceDirect

Infrared Physics & Technology 50 (2007) 217–226

INFRARED PHYSICS & TECHNOLOGY

www.elsevier.com/locate/infrared

Towards dualband megapixel QWIP focal plane arrays

S.D. Gunapala [a,*], S.V. Bandara [a], J.K. Liu [a], J.M. Mumolo [a], C.J. Hill [a], S.B. Rafol [b], D. Salazar [c], J. Woolaway [c], P.D. LeVan [d], M.Z. Tidrow [e]

[a] *Jet Propulsion Laboratory, California Institute of Technology, Pasadena, CA 91109, USA*

[b] *Infravision Systems, 2400 Lincoln Avenue, Altadena, CA 91001, USA*

[c] *FLIR Systems Inc., Indigo Operations, 70 Castilian Dr., Goleta, CA 93117, USA*

[d] *Air Force Research Laboratory, Kirtland Air Force Base, NM 87117, USA*

[e] *Missile Defense Agency/AS, 7100 Defense Pentagon, Washington, DC 20301, USA*

Available online 8 December 2006

Abstract

Mid-wavelength infrared (MWIR) and long-wavelength infrared (LWIR) 1024×1024 pixel quantum well infrared photodetector (QWIP) focal planes have been demonstrated with excellent imaging performance. The MWIR QWIP detector array has demonstrated a noise equivalent differential temperature (NEΔT) of 17 mK at a 95 K operating temperature with *f*/2.5 optics at 300 K background and the LWIR detector array has demonstrated a NEΔT of 13 mK at a 70 K operating temperature with the same optical and background conditions as the MWIR detector array after the subtraction of system noise. Both MWIR and LWIR focal planes have shown background limited performance (BLIP) at 90 K and 70 K operating temperatures respectively, with similar optical and background conditions. In addition, we have demonstrated MWIR and LWIR pixel co-registered simultaneously readable dualband QWIP focal plane arrays. In this paper, we will discuss the performance in terms of quantum efficiency, NEΔT, uniformity, operability, and modulation transfer functions of the 1024×1024 pixel arrays and the progress of dualband QWIP focal plane array development work.

Keywords: Infrared detectors; Quantum wells; QWIP; Dualband; Two-color; Multi-band; Infrared imaging; Focal plane arrays

1. MWIR QWIP device

A quantum well structure designed to detect infrared (IR) light is commonly referred to as a quantum well infrared photodetector (QWIP). An elegant candidate for the QWIP is the square quantum well of basic quantum mechanics [1,2]. A coupled-quantum well structure was used in this device to broaden the responsivity spectrum. In the MWIR device described here, each period of the multi-quantum-well (MQW) structure consists of coupled quantum wells of 40 Å containing 10 Å GaAs, 20 Å $In_{0.3}Ga_{0.7}As$, and 10 Å GaAs layers (doped $n = 1 \times 10^{18}\ cm^{-3}$) and a 40 Å undoped barrier of $Al_{0.3}Ga_{0.7}As$ between coupled quantum wells, and a 400 Å thick undoped barrier of $Al_{0.3}Ga_{0.7}As$. Stacking many identical periods (typically 50) together increases photon absorption. Ground state electrons are provided in the detector by doping the GaAs well layers with Si (see Fig. 1). This photosensitive MQW structure is sandwiched between 0.5 μm GaAs top and bottom contact layers doped $n = 5 \times 10^{17}\ cm^{-3}$, grown on a semi-insulating GaAs substrate by molecular beam epitaxy (MBE). Then a 0.7 μm thick GaAs cap layer on top of a 300 Å $Al_{0.3}Ga_{0.7}As$ stop-etch layer was grown *in situ* on top of the device structure to fabricate the light coupling optical cavity [3–12].

The MBE grown material was tested for absorption efficiency using a Fourier Transform Infrared (FTIR) spectrometer. The experimentally measured peak absorption (or internal) quantum efficiency (η_a) of this material at room temperature was 19%. A detail description on quantum efficiency measurements can be found elsewhere [6]. Due to the fact that the n–i–n QWIP device is a photoconductive device, the net (or external) quantum efficiency

* Corresponding author.
E-mail address: sarath.d.gunapala@jpl.nasa.gov (S.D. Gunapala).

1350-4495/$ - see front matter
doi:10.1016/j.infrared.2006.10.005

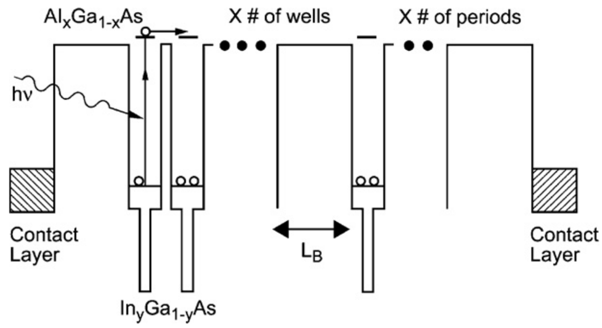

Fig. 1. Schematic diagram of the conduction band in a bound-to-quasibound QWIP. A couple quantum well structure has been used to broaden the responsivity spectrum.

η can be determined using $\eta = \eta_a \cdot g$, where g is the photoconductive gain of the detector. The epitaxially grown material was processed into 200 μm diameter mesa test structures (area $= 3.14 \times 10^{-4}$ cm^2) using wet chemical etching, and Au/Ge ohmic contacts were evaporated onto the top and bottom contact layers. The detectors were back illuminated through a 45° polished facet [5–7] and a responsivity spectrum is shown in Fig. 2. The responsivity of the detector peaks at 4.6 μm and the peak responsivity (R_p) of the detector is 170 mA/W at bias $V_B = -1$ V. The spectral width and the cutoff wavelength are $\Delta\lambda/\lambda = 15\%$ and $\lambda_c = 5.1$ μm respectively. The photoconductive gain, g, was experimentally determined using [13] $g = i_n^2/4eI_DB + 1/2N$, where B is the measurement bandwidth, N is the number of quantum wells, and i_n is the current noise, which was measured using a spectrum analyzer. The photoconductive gain of the detector was 0.23 at $V_B = -1$ V and reached 0.98 at $V_B = -5$ V. Since the gain of a QWIP is inversely proportional to the number of quantum wells N, the better comparison would be the well capture probability p_c, which is directly related to the gain [13] by $g = 1/Np_c$. The calculated well capture probabilities are 25% at low bias (i.e., $V_B = -1$ V) and 2% at high bias

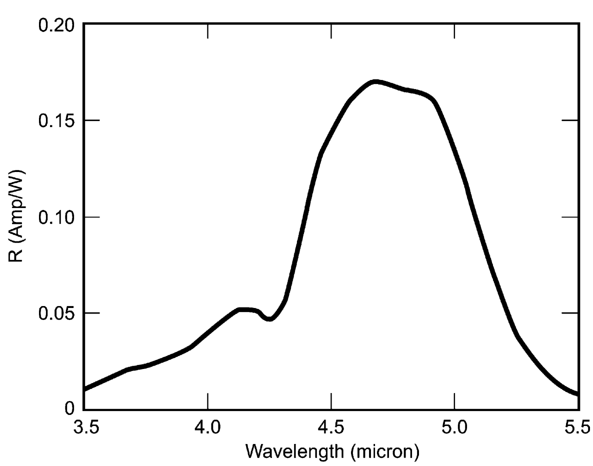

Fig. 2. Responsivity spectrum of a bound-to-quasibound MWIR QWIP test structure at temperature $T = 77$ K. The spectral response peak is at 4.6 μm and the long wavelength cutoff is at 5.1 μm.

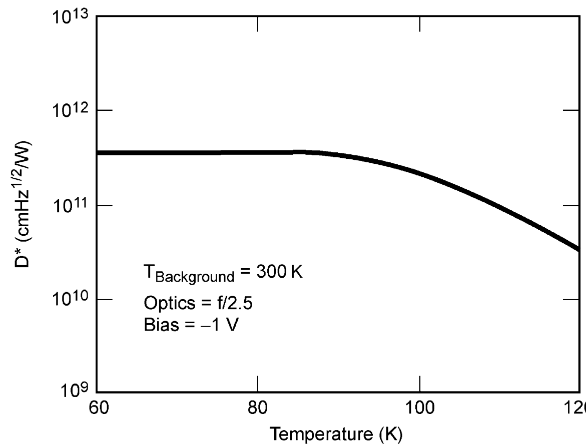

Fig. 3. Detectivity as a function of detector operating temperature at bias of $V_B = -1$ V.

(i.e., $V_B = -5$ V), which together indicate the excellent hot-electron transport in this device structure. The peak net quantum efficiency was determined using $\eta = \eta_a \cdot g$. Thus, the net peak quantum efficiency at bias $V_B = -1$ V is 4.6%. The lower quantum efficiency is due to the lower photoconductive gain at lower operating bias. A lower operating bias is used to suppress the detector dark current. Due to a low readout multiplexer well depth (i.e., 8×10^6 electrons) a lower dark current is mandatory to achieve a higher operating temperature and longer integration times. In background limited performance (BLIP) conditions the noise equivalent differential temperature (NEΔT) improves with increasing integration time. However, the absorption quantum efficiency can be increased further up to 60–70% with higher quantum well doping densities. As a result, the operating temperature of the devices will decrease [9].

The peak detectivity is defined as $D_P^* = R_P\sqrt{AB}/i_n$, where R_P is the peak responsivity, A is the area of the detector and $A = 3.14 \times 10^{-4}$ cm^2. The measured peak detectivity at bias $V_B = -1$ V and temperature $T = 90$ K is 4×10^{11} cm $\sqrt{\text{Hz}}$/W. Fig. 3 shows the peak detectivity as a function of detector operating temperature at bias $V_B = -1$ V. These detectors show BLIP at a bias $V_B = -1$ V and temperature $T = 90$ K for 300 K background with f/2.5 optics.

2. 1024 × 1024 pixel MWIR QWIP focal plane array

It is well known that QWIPs do not absorb radiation incident normal to the surface unless the infrared radiation has an electric field component normal to the layers of the superlattice (growth direction) [6]. Thus, various light coupling techniques, such as 45° edge coupling, random reflectors, corrugated surfaces [14], two-dimensional grating structures [15], etc. have been used to couple normal incidence infrared radiation into QWIPs. Although random reflectors have achieved relatively high quantum efficiencies with large test device structures, it is not possible to achieve the similar high quantum efficiencies with random reflectors on small focal plane array (FPA) pixels due to the reduced width-to-height aspect ratios. In addition, it is difficult to fabricate random reflectors for shorter wavelength detectors relative to very long-wavelength detectors (i.e., 15 μm) due to the fact that feature sizes of random reflectors are linearly proportional to the peak wavelength of the detectors. For example, the minimum feature size of the random reflectors of 15 μm cutoff and 5 μm cutoff FPAs were 1.25 and 0.3 μm respectively and it is difficult to fabricate sub-micron features by contact photolithography [16].

As a result, the random reflectors of the 5 μm cutoff FPA were less sharp and had fewer scattering centers compared to the random reflectors of the 15 μm cutoff QWIP FPA. As we have discussed previously [5,6,15], additional infrared light can be coupled to the QWIP detector structure by incorporating a two-dimensional grating surface on top of the detectors, which also removes the light coupling limitations and makes two-dimensional QWIP imaging arrays feasible. This two-dimensional grating structure was fabricated on the detectors by using standard photolithography and CCl_2F_2 selective dry etching.

After the two-dimensional grating array was defined by lithography and dry etching, the photoconductive QWIPs of the 1024×1024 FPAs were fabricated by dry chemical etching through the photosensitive $GaAs/Al_xGa_{1-x}As$ MQW layers into the 0.5 μm thick doped GaAs bottom contact layer. The pitch of the FPA is 19.5 μm and the actual pixel size is $17.5 \times 17.5\ \mu m^2$. The two-dimensional gratings on top of the detectors were then covered with Au/Ge and Au for Ohmic contacts and high reflectivity. Fig. 4 shows nine processed 1024×1024 QWIP FPAs on a 4 in. GaAs wafer. Indium bumps were then evaporated on top of the detectors for a silicon CMOS readout integrated circuit (ROIC) hybridization process. A few QWIP FPAs were chosen and hybridized (via an indium bump-bonding process) to a 1024×1024 silicon CMOS ROICs and biased at $V_B = -1$ V. At temperatures below 90 K, the signal to noise ratio of the system is limited by array non-uniformity, ROIC readout noise, and photo current (photon flux) noise. At temperatures above 90 K, temporal noise due to the QWIP's higher dark current becomes the limitation. As mentioned earlier this higher dark current is due to thermionic emission and thus causes the charge storage capacitors of the readout circuitry to saturate. Since the QWIP is a high impedance device, it should yield a very high charge injection coupling efficiency into the integration capacitor of the multiplexer. In fact, Gunapala et al. [17] have demonstrated charge injection efficiencies approaching 90%. Charge injection efficiency can be obtained from [7,8,16], as

$$\eta_{inj} = \frac{g_m R_{Det}}{1 + g_m R_{Det}} \left[\frac{1}{1 + \frac{j\omega C_{Det} R_{Det}}{1 + g_m R_{Det}}} \right] \quad (1)$$

where g_m is the transconductance of the MOSFET and is given by $g_m = eI_{Det}/kT$. The differential resistance R_{Det} of the pixels at -1 V bias is $6.3 \times 10^{12}\ \Omega$ at $T = 85$ K and detector capacitance C_{Det} is 2.0×10^{-14} F. The detector dark current $I_{Det} = 0.1$ pA under the same operating conditions. According to Eq. (1) the charge injection efficiency is $\eta_{inj} = 98.8\%$ at a frame rate of 10 Hz. The FPA was back-illuminated through the flat thinned substrate membrane (thickness 800 Å). This initial array gave excellent images with 99.95% of the pixels working (number of dead pixels 500), demonstrating the high yield of GaAs technology. The operability was defined as the percentage of pixels having noise equivalent differential temperature less than 100 mK at 300 K background and in this case operability happens to be equal to the pixel yield.

We have used the following equation to calculate the noise equivalent differential temperature NEΔT of the FPA:

$$\text{NE}\Delta\text{T} = \frac{\sqrt{AB}}{D_B^*(dP_B/dT)\sin^2(\theta/2)} \quad (2)$$

where D_B^* is the blackbody detectivity, dP_B/dT is the derivative of the integrated blackbody power with respect to temperature, and θ is the field of view angle [i.e., $\sin^2(\theta/2)=(4f^2+1)^{-1}$, where f is the f number of the optical system]. Fig. 5 shows the NEΔT of the FPA estimated from test structure data as a function of temperature for bias voltages $V_B = -1$ V. The background temperature $T_B = 300$ K, the area of the pixel $A=(17.5 \times 17.5\ \mu m^2)$, the f number of the optical system is 2.5, and the frame rate is 10 Hz. Fig. 6 shows the measured NEΔT of the imaging system at an operating temperature of $T = 90$ K, 60 ms integration time, bias $V_B = -1$ V for 300 K background with $f/2.5$ optics and the mean value is 23 mK. This agrees well with our estimated value of 15 mK based on test structure data (see Fig. 5). It is worth noting that the NEΔT of the detector array is reduced to 17 mK after removing the noise factors associate with ROIC, electronics, etc. The net peak quantum efficiency of the FPA was 3.8% (lower focal plane array quantum efficiency is attributed to lower photoconductive gain at lower operating bias and lower well doping densities used in this device structure) and this corresponds to an average of three passes of infrared radiation

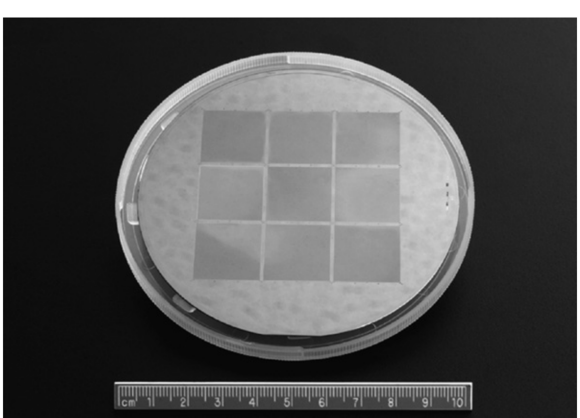

Fig. 4. Nine 1024×1024 QWIP focal plane arrays on a 4 in. GaAs wafer.

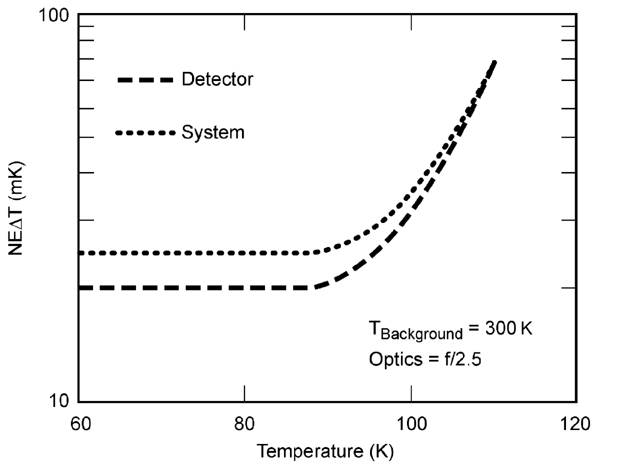

Fig. 5. Noise equivalent differential temperature NEΔT estimated from test structure data as a function of temperature for bias voltage $V_B = -2$ V. The background temperature $T_B = 300$ K and the area of the pixel $A = (17.5\ \mu m)^2$.

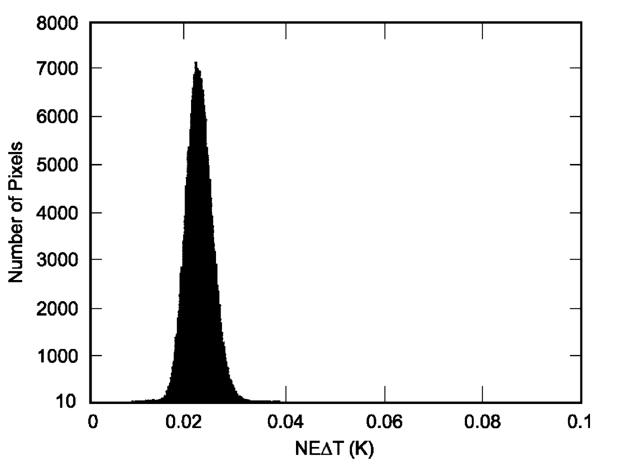

Fig. 6. NEΔT histogram of the 1,048,576 pixels of the 1024 × 1024 array showing a high uniformity of the FPA. The uncorrected non-uniformity (= standard deviation/mean) of the FPA is only 5.5% including 1% non-uniformity of ROC and 1.4% non-uniformity due to the cold-stop not being able to give the same field of view to all the pixels in the FPA. As shown in this figure, the measured NEΔT of the MWIR 1 K × 1 K QWIP camera is 23 mK. The noise of the camera system can be written as, $N^2_{SYS} = n^2_{Detector} + n^2_{ADC} + n^2_{MUX}$, where $n_{Detector}$ is the noise of the FPA, n_{ADC} is the noise of the analog-to-digital converter, and n_{MUX} is the noise of the silicon ROIC. The experimentally measured N_{SYS} is 2 units, and the n_{ADC} and n_{MUX} are 0.8 and 1 unit, respectively. This yields 1.5 noise units for $n_{Detector}$. Thus, the NEΔT of the FPA is 17 mK at 300 K background with *f*/2.5 optics and 60 ms integration time. This agrees reasonably well with our estimated value of 20 mK based on test detector data (see Fig. 5).

(equivalent to a single 45° pass) through the photosensitive MQW region. It is worth noting that under BLIP conditions the performance of the detectors is independent of the photoconductive gain, and it depends only on the absorption quantum efficiency.

A 1024 × 1024 QWIP FPA hybrid was mounted onto a 5 W integral Sterling closed-cycle cooler assembly to demonstrate a portable MWIR camera. The digital acquisition resolution of the camera is 14-bits, which determines the

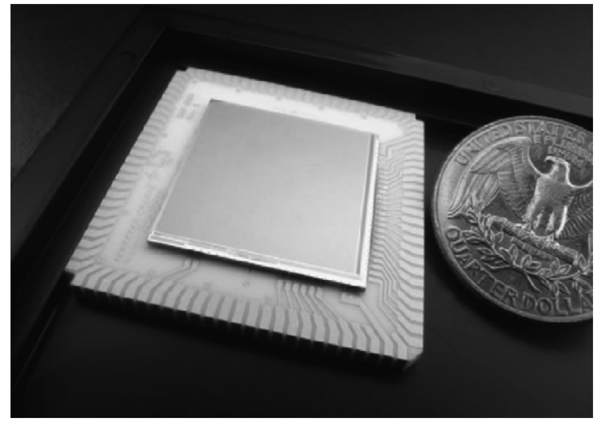

Fig. 7. Picture a 1024 × 1024 pixel QWIP focal plane array mounted on a 84-pin lead less chip carrier.

instantaneous dynamic range of the camera (i.e., 16,384). However, the dynamic range of QWIP is 85 DB. The preliminary data taken from a test set up has shown mean system NEΔT of 22 mK (the higher NEΔT is due to the 65% transmission through the lens assembly, and system noise of the measurement setup) at an operating temperature of $T = 90$ K and bias $V_B = -1$ V, for a 300 K background. It is worth noting that these data were taken from the first 1024 × 1024 QWIP FPA which we have produced. Thus, we believe that there is a plenty of room for further improvement of these FPAs.

A 1024 × 1024 QWIP FPA hybrid (see Fig. 7) was mounted onto a 5 W integral Sterling closed-cycle cooler assembly to demonstrate a portable MWIR camera. The digital acquisition resolution of the camera is 14-bits, which determines the instantaneous dynamic range of the camera (i.e., 16,384). However, the dynamic range of QWIP is 85 DB. The preliminary data taken from a test set up has shown mean system NEΔT of 22 mK (the higher NEΔT is due to the 65% transmission through the lens assembly, and system noise of the measurement setup) at an operating temperature of $T = 90$ K and bias $V_B = -1$ V, for a 300 K background. It is worth noting that these data were taken from the first 1024 × 1024 QWIP FPA which we have produced. Thus, we believe that there is a plenty of room for further improvement of these FPAs.

Video images were taken at a frame rate of 10 Hz at temperatures as high as $T = 90$ K, using a ROIC capacitor having a charge capacity of 8×10^6 electrons (the maximum number of photoelectrons and dark electrons that can be counted in the time taken to read each detector pixel). Fig. 8 shows one frame of a video image taken with a 5.1 μm cutoff 1024 × 1024 pixel QWIP camera.

3. LWIR QWIP device

Each period of this LWIR MQW structure consists of quantum wells of 40 Å and a 600 Å barrier of $Al_{0.27}Ga_{0.73}As$. As mentioned earlier, stacking many iden-

Fig. 8. One frame of video image taken with the 5.1 μm cutoff 1024 × 1024 pixel QWIP camera.

tical periods (the device in this study has 50 periods) together increases photon absorption. Ground state electrons are provided in the detector by doping the GaAs well layers with silicon impurities up to $n = 5 \times 10^{17}$ cm^{-3}. This photosensitive MQW structure is sandwiched between 0.5 μm GaAs top and bottom contact layers doped $n = 5 \times 10^{17}$ cm^{-3}, grown on a semi-insulating GaAs substrate by MBE. Then a 0.7 μm thick GaAs cap layer on top of a 300 Å $Al_{0.27}Ga_{0.73}As$ stop-etch layer was grown *in situ* on top of the device structure to fabricate the light coupling optical cavity [2–5].

The MBE grown material was tested for absorption efficiency using a FTIR spectrometer. Test detectors with a 200 μm diameter were fabricated and back-illuminated through a 45° polished facet [6] for optical characterization and an experimentally measured responsivity spectrum is shown in Fig. 9. The responsivity of the detector peaks at

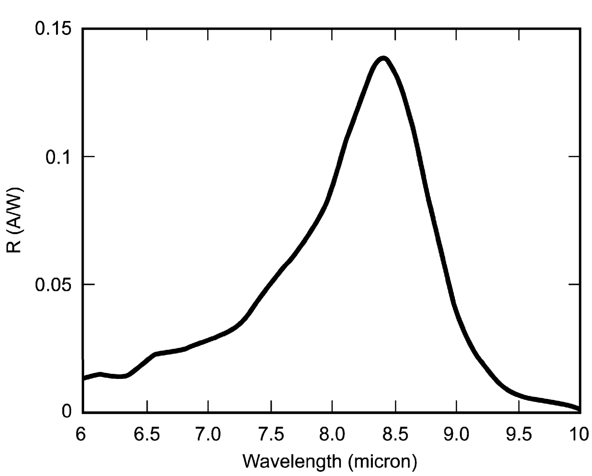

Fig. 9. Responsivity spectrum of a bound-to-quasibound LWIR QWIP test structure at temperature $T = 77$ K. The spectral response peak is at 8.4 μm and the long wavelength cutoff is at 8.8 μm.

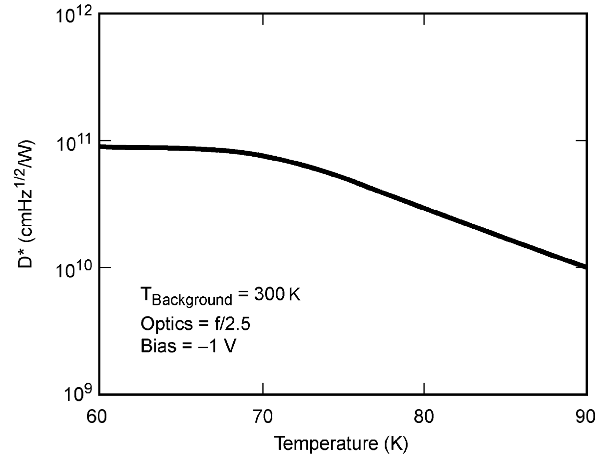

Fig. 10. Detectivity as a function of temperatures at bias of −1 V.

8.4 μm and the peak responsivity (R_P) of the detector is 130 mA/W at bias $V_B = -1$ V. The spectral width and the cutoff wavelength are $\Delta\lambda/\lambda = 10\%$ and $\lambda_c = 8.8$ μm, respectively.

The photoconductive gain g was experimentally determined as described in the previous section. The peak detectivity of the LWIR detector was calculated using experimentally measured noise current i_n. The calculated peak detectivity at bias $V_B = -1$ V and temperature $T = 70$ K is 1×10^{11} cm$\sqrt{\text{Hz}}$/W (see Fig. 10). These detectors show BLIP at bias $V_B = -1$ V and temperature $T = 72$ K for a 300 K background with *f*/2.5 optics.

4. 1024 × 1024 pixel LWIR QWIP focal plane array

A light coupling two-dimensional grating structure was fabricated on the detectors by using standard photolithography and CCl_2F_2 selective dry etching. After the two-dimensional grating array was defined by lithography and dry etching, the photoconductive QWIPs of the 1024 × 1024 FPAs were fabricated by dry chemical etching through the photosensitive $GaAs/Al_xGa_{1-x}As$ MQW layers into the 0.5 μm thick doped GaAs bottom contact layer as described earlier. The pitch of the FPA is 19.5 μm and the actual pixel size is 17.5 × 17.5 μm^2. The two-dimensional gratings on top of the detectors were then covered with Au/Ge and Au for Ohmic contacts and high reflectivity. Nine 1024 × 1024 pixel QWIP FPAs were processed on a 4-in. GaAs wafer. Indium bumps were then evaporated on top of the detectors for hybridization with silicon CMOS ROICs. A single QWIP FPA was chosen and hybridized (via indium bump-bonding process) to a 1024 × 1024 CMOS multiplexer and biased at $V_B = -1$ V. At temperatures below 72 K, the signal-to-noise ratio of the system is limited by array non-uniformity, ROIC readout noise, and photocurrent (photon flux) noise. At temperatures above 72 K, the temporal noise due to the dark current becomes the limitation. The differential resistance R_{Det} of the pixels at −1 V bias is 7.4×10^{10} Ω at

$T = 70$ K and detector capacitance C_{Det} is 1.7×10^{-14} F. The detector dark current $I_{\text{Det}} = 1.6$ pA under the same operating conditions. The charge injection efficiency into the ROIC was calculated as described in earlier section. An average charge injection efficiency of $\eta_{\text{inj}} = 95\%$ has been achieved at a frame rate of 30 Hz. It is worth noting that, the charge injection efficiency gets closer to one, especially when photocurrent is present. Since we are using direct injection ROIC, the injection efficiency gets better at higher drain current or when there is more photocurrent. Charge injection efficiency becomes worst at very low background flux, but limited by dark current for QWIP detector, i.e., the dark current keeps the pixel on. This initial array gave excellent images with 99.98% of the pixels working (number of dead pixels 200), again demonstrating the high yield of GaAs technology.

NEΔT of the FPA was calculated using Eq. (2). Fig. 11 shows the NEΔT of the FPA estimated from test structure data as a function of temperature for a bias voltage $V_B = -1$ V. The background temperature $T_B = 300$ K, the area of the pixel $A = (17.5 \times 17.5\ \mu\text{m}^2)$, the f number of the optical system is 2.5, and the frame rate is 30 Hz. Fig. 12 shows the measured NEΔT of the system at an operating temperature of $T = 72$ K, 29 ms integration time, bias $V_B = -1$ V for 300 K background with $f/2.5$ optics and the mean value is 16 mK. The noise of the camera system can be written as, $N_{\text{SYS}}^2 = n_{\text{Detector}}^2 + n_{\text{ADC}}^2 + n_{\text{MUX}}^2$, where n_{Detector} is the noise of the FPA, n_{ADC} is the noise of the analog-to-digital converter, and n_{MUX} is the noise of the silicon ROIC. The experimentally measured N_{SYS} is 2.4 units, and the n_{ADC} and n_{MUX} are 0.8 and 1 unit, respectively. This yields 2.0 noise units for n_{Detector}. Thus, the NEΔT of the detector array is 13 mK at 300 K background with $f/2.5$ optics and 29 ms integration time. This agrees reasonably well with our estimated value of 15 mK based on test detector data (see Fig. 11).

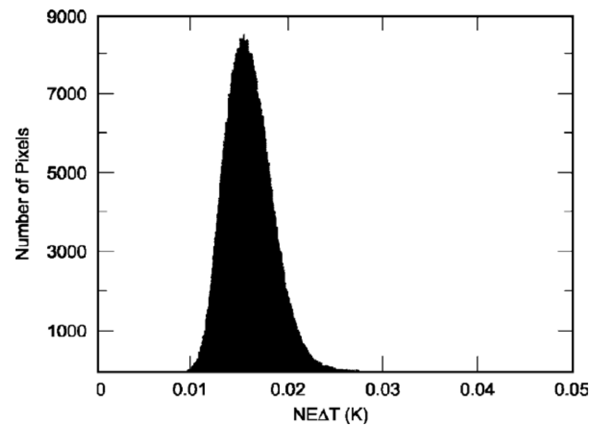

Fig. 12. NEΔT histogram of the 1,048,576 pixels of the 1024 × 1024 array showing a high uniformity of the FPA. The uncorrected non-uniformity (=standard deviation/mean) of the FPA is only 8% including 1% non-uniformity of ROC and 4% non-uniformity due to the cold-stop and optics not being able to give the same field of view to all the pixels in the FPA. As shown in this figure, after single-point correction non-uniformity reduced to 0.8%.

A 1024 × 1024 QWIP FPA hybrid was mounted onto a 5 W integral Sterling closed-cycle cooler assembly to demonstrate a portable LWIR camera. The digital data acquisition resolution of the camera is 14-bits, which determines the instantaneous dynamic range of the camera (i.e., 16,384). The preliminary data taken from a test set up has shown mean system NEΔT of 16 mK at an operating temperature of $T = 72$ K and bias $V_B = -1$ V, for a 300 K background.

Video images were taken at a frame rate of 30 Hz at temperatures as high as $T = 72$ K, using a ROIC capacitor having a charge capacity of 8×10^6 electrons. Fig. 13 shows one frame of a video image taken with a 9 μm cutoff 1024 × 1024 pixel QWIP camera. In addition, the minimum resolvable temperature difference was measured by a single

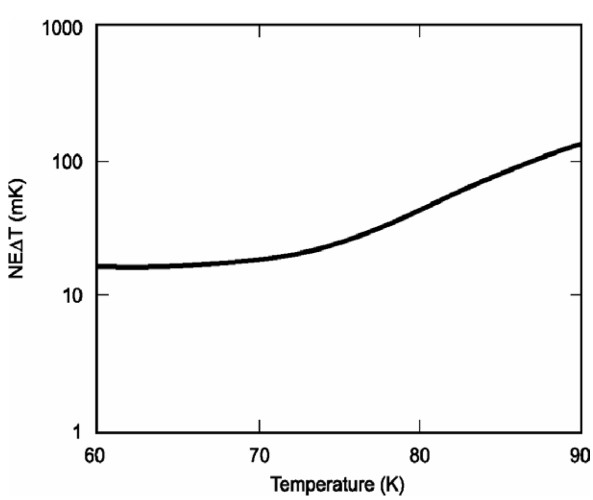

Fig. 11. Noise equivalent temperature difference NEΔT estimated from test structure data as a function of temperature for bias voltage $V_B = -2$ V. The background temperature $T_B = 300$ K, optics $f = 2.5$, and the area of the pixel $A = (17.5\ \mu\text{m})^2$.

Fig. 13. One frame of video image taken with the 9 μm cutoff 1024 × 1024 pixel QWIP camera.

observer using seven bar targets ranging in spatial frequency from 0.1 cycles/mrad up to 1.33 cy/mrad, which was the first target where no contrast could be measured (unclear). While the collection of the data does not adhere to the generally accepted requirements of having multiple observers, the data is consistent with the NEΔT measurement and worth reporting. At the lowest spatial frequency, the minimum resolvable differential temperature (MRDT) was 16 mK.

It is worth noting that these data were taken from the first 1024 × 1024 QWIP FPAs we produced. Thus, we believe that there is a plenty of room for further improvement of these FPAs. For example, an implementation of an enhanced optical cavity designed using transmission-line techniques with the electromagnetic boundary conditions as described by Lin et al. [18] will further improve the net quantum efficiency and the signal-to-noise-ratio of these devices. Furthermore, using the InGaAs/InP material system may improve the photoconductive gain significantly [19]. This will allow QWIP device structure to have more than the typical 50-periods without significant degradation in photoconductive gain. This will also increase the net quantum efficiency of the QWIPs. Together with high FPA uniformity, high operability, negligible pixel-to-pixel optical cross-talk, low $1/f$ noise [6], and possible high quantum efficiency, QWIP FPAs will be attractive to both spaceborne and terrestrial infrared applications.

5. MWIR and LWIR dualband QWIP focal plane arrays

There are many applications that require MWIR and LWIR dualband FPAs. For example, a dualband FPA camera would provide the absolute temperature of a target with unknown emissivity, which is extremely important to the process of identifying a temperature difference between missile targets, warheads, and decoys. Dualband infrared FPAs can also play many important roles in Earth and planetary remote sensing, astronomy, etc. Furthermore, monolithically integrated pixel collocated simultaneously readable dualband FPAs eliminate the beam splitters, filters, moving filter wheels, and rigorous optical alignment requirements imposed on dualband systems based on two separate single-band FPAs or a broadband FPA system with filters. Dualband FPAs also reduce the mass, volume, and power requirements of dualband systems. Due to the inherent properties such as narrow-band response, wavelength tailorability, and stability (i.e., low $1/f$ noise) associated with GaAs based QWIPs [1–6], it is an ideal candidate for large format dualband infrared FPAs. In this section, we discuss the development of a 320 × 256 pixel MWIR and LWIR pixel colocated simultaneously readable dualband QWIP FPA.

As shown in Fig. 14, our dualband FPA is based on a two different types of (i.e., MWIR and LWIR; see Fig. 15 for the responsivity spectrums) QWIP devices separated by a 0.5 μm thick, heavily doped, n-type GaAs layer. The device structures of the MWIR and LWIR

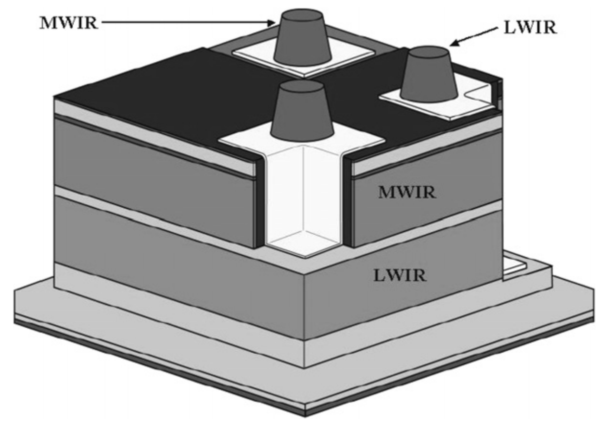

Fig. 14. 3-D view of dualband QWIP device structure showing via connects for independent access of MWIR and LWIR devices.

devices are very similar to the MWIR and LWIR devices described earlier in this paper. Both device structures and heavily doped contact layers were grown in situ during a single growth run using molecular beam epitaxy. It is worth noting that the photosensitive MQW region of each QWIP device is transparent at other wavelengths, which is an important advantage over conventional interband detectors. This spectral transparency makes QWIPs ideally suited for dualband FPAs with negligible spectral cross-talk. As shown in Fig. 14, the carriers emitted from each MWQ region are collected separately using three contacts. The middle contact layer is used as the detector common. The electrical connections to the detector common, and the LWIR pixel connection, are brought to the top of each pixel using via connections. The first dualband QWIP FPA with pixel collocation and simultaneous operation in MWIR and LWIR has been described by Glodberg et al. [20]. This 256 × 256 pixel dualband FPA has achieved a NEΔT of 30 mK in the MWIR spectral band and 34 mK in the LWIR spectral band.

Light coupling to a pixel collocated dualband QWIP device is a challenge since each device has only a single top surface area. We have developed two different optical coupling techniques. The first technique uses a dual period Lamar grating structure. The second technique uses the multiple diffraction orders. In this light coupling technique,

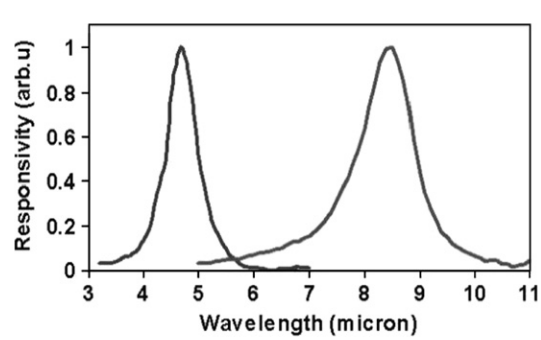

Fig. 15. Responsivity of the dualband QWIP device as a function of wavelength.

we have used a 2-D grating with single pitch. The first diffraction orders $(1,0)$, $(0,1)$, $(-1,0)$, and $(0,-1)$ couple infrared radiation into LWIR pixels, and the second diffraction orders $(1,1)$, $(-1,1)$, $(1,-1)$, and $(-1,-1)$ couple infrared radiation into MWIR pixels. The spectral responsivity of dualband QWIP is shown in Fig. 19. 2-D periodic grating structures were designed to couple the 4–5 and 8–9 μm radiation into the detector pixels. The top 0.7 μm thick GaAs cap layer was used to fabricate the light coupling 2-D periodic grating. The 2-D grating reflectors on top of the detectors were then covered with Au/Ge and Au for Ohmic contact and reflection.

After the 2-D grating array was defined by photolithography and dry etching, the MWIR detector pixels of the 320×256 pixel FPAs, and the via hole to access the detector common, were fabricated by dry etching through the photosensitive GaAs/$In_yGa_{1-y}As$/$Al_xGa_{1-x}As$ MQW layers into the 0.5 μm thick doped GaAs intermediate contact layer. Then LWIR pixels and via holes to access the LWIR pixels of FPAs were fabricated. A thick insulation layer was deposited and contact windows were opened at the bottom of each via hole and on top surface. Ohmic contact metal was evaporated and unwanted metal was removed using a metal lift-off process. The pitch of the FPA is 40 μm and the actual MWIR and LWIR pixel sizes are $38 \times 38\ \mu m^2$. Fig. 16 shows a SEM picture of a corner of one dualband QWIP pixel, which clearly shows via holes and metal connects used to bring the electrical contacts to the top surface of the detector pixels. Forty eight FPAs were processed on a 4-in. GaAs wafer. Indium bumps were then evaporated on top of the detectors for silicon read out integrated circuit (ROIC) hybridization. Several dualband FPAs were chosen and hybridized (via an indium bump-bonding process) to a 320×256 pixel CMOS read out integrated circuit (ISC-0006). Fig. 17 shows a FPA hybrid.

A selected MWIR:LWIR pixel co-registered simultaneously readable dualband QWIP FPA has been mounted on to the cold finger of a reusable dewar, cooled by a Stirlin cycle cooler and the two bands (i.e., MWIR and LWIR) were independently biased. At temperatures below 68 K, the signal to noise ratio of the system is limited by array non-uniformity, ROIC readout noise, and photo current (photon flux) noise. At temperatures above 72 K, temporal noise due to the LWIR QWIP's higher dark current becomes the limitation. Since the QWIP is a high impedance device, it should yield a very high charge injection coupling efficiency into the integration capacitor of the multiplexer. In fact, Gunapala et al. [7,8] have demonstrated charge injection efficiencies approaching 90%. The FPA was back-illuminated through the flat thinned substrate membrane (thickness 500 Å). This initial array gave good images with 95% of the pixels working, which is excellent compared to the difficultness in the fabrication process of this pixel co-registered simultaneously readable dualband QWIP FPA. The operability was defined as the percentage of pixels having NEΔT within 3σ of the NEΔT histograms taken at 300 K background with $f/2$ cold shield.

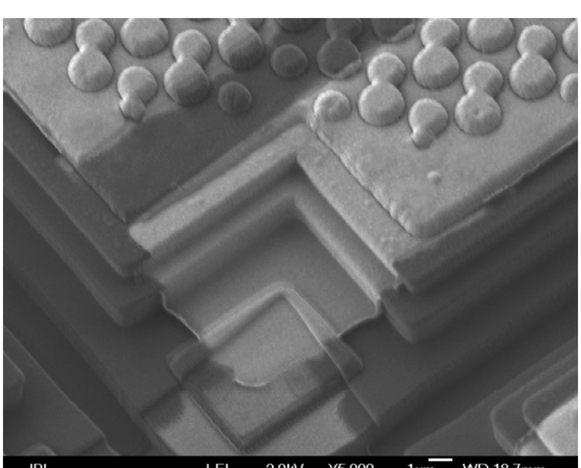

Fig. 16. SEM picture of a dual band via connection.

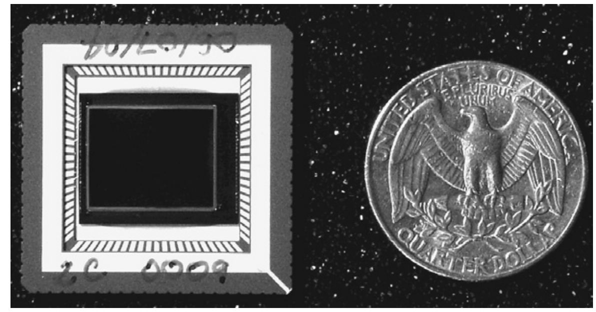

Fig. 17. Picture a 320×256 pixel dualband QWIP FPA mounted on a 84-pin lead less chip carrier.

A 320×256 pixel co-registered simultaneously readable dualband QWIP FPA hybrid was mounted onto a 5 W integral Sterling closed-cycle cooler assembly to demonstrate a portable MWIR:LWIR dualband QWIP camera. The digital acquisition resolution of the camera is 14-bits, which determines the instantaneous dynamic range of the camera (i.e., 16,384). However, the dynamic range of QWIP is 85 DB. Video images were taken at a frame rate of 30 Hz at temperatures as high as $T = 68$ K, using two ROIC capacitors having a charge capacities of 21×106 and 87×106 electrons for the MWIR and LWIR bands respectively. Fig. 18 shows an image taken with the 320×256 pixel co-registered simultaneously readable MWIR:LWIR dualband QWIP camera. The person in this image is holding a cigarette lighter. The cigarette lighter produced a lot of hot CO_2 gas. Thus, the flame in the MWIR image looks broader due to re- emission of infrared signal in the 4.1–4.3 μm band by the heated CO_2 gas produced by the cigarette lighter. Whereas, heated CO_2 gas does not have any emission lines in the LWIR (8–9 μm) band. Thus, LWIR image shows only thermal signatures of the flame. The hot cigarette lighter flame produced a lot of MWIR signal, so it reflects off from the lens and face.

As expected (due to BLIP), the estimated and experimentally obtained NEΔT values of the LWIR detectors

Fig. 18. An image taken with the 320 × 256 pixel co-registered simultaneously readable MWIR:LWIR dualband QWIP camera. The person in this image is holding a cigarette lighter. The cigarette lighter produced lots of hot CO_2 gas. So, flame in MWIR image looks broader due to re-emission of infrared signal in 4.1–4.3 μm band by the heated CO_2 gas produced by the cigarette lighter. Whereas, heated CO_2 gas does not have any emission line in the LWIR (8–9 μm) band. Thus, LWIR image shows only thermal signatures of the flame. The hot cigarette lighter flame produced a lot of MWIR signal, so it reflects off from the lens and face.

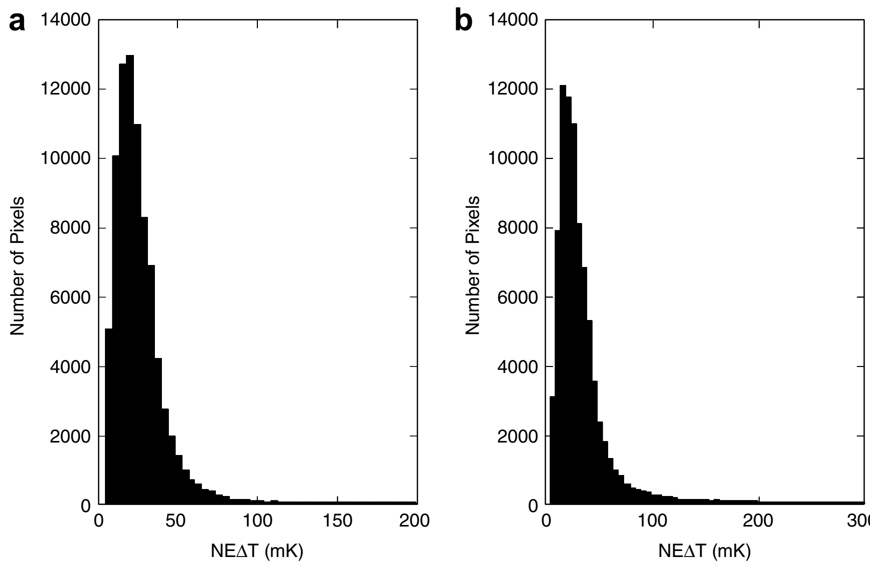

Fig. 19. NEΔT histogram of the 320 × 256 format simultaneously readable pixel co-registered dualband QWIP focal plane array. Each spectral band of the FPA consisted of 320 × 256 co-registered pixels. The experimentally measured NEΔT of MWIR and LWIR detectors at 65 K are 28 and 38 mK, respectively.

do not change significantly at temperatures below 65 K. The estimated NEΔT of MWIR and LWIR detectors at 65 K are 22 and 24 mK, respectively. These estimated NEΔT values based on the test detector data agree reasonably well with the experimentally obtained values. The experimentally measured NEΔT values are shown in Fig. 19(a) and (b). The experimentally measured NEΔT values are slightly higher than the estimated NEΔT value based on the results of single element test detector data. This degradation in signal-to-noise ratio is attributed to the inefficient light coupling of the dual feature lamallar grating coupler, unoptimized ROIC, and the significant amount of $1/f$ noise in the FPA characterization equipment.

As we have mentioned earlier, QWIP is an ideal detector for the fabrication of pixel co-registered simultaneously readable dualband infrared focal plane arrays, because, QWIP absorbs infrared radiation only in a narrow spectral band which is designed to do so, and transparent outside of that absorption (i.e., detection) band. Thus it provides zero spectral cross-talk when two spectral bands are a few microns apart. The initial GaAs substrate of these dualband FPAs are completely removed leaving only a 50 nm thick GaAs membrane. Thus, these dualband QWIP FPAs are not vulnerable to FPA delamination and indium bump breakage during thermal recycling process, and has zero pixel-to-pixel optical cross-talk. Inspired from this success, now we are developing a megapixel (1024 × 1024 pixel) dualband QWIP FPA sensitive in MWIR and LWIR spectral bands.

Acknowledgements

Authors are grateful to P. Dimotakis, S. Forouhar, P. Grunthaner, T. Krabach, A. Larson, R. Liang, T. Luchik, and R. Stirbl for encouragement and support during the development and optimization of QWIP FPAs at the Jet Propulsion Laboratory for various applications. The research described in this paper was performed by the Jet Propulsion Laboratory, California Institute of Technology, and was sponsored by the Missile Defense Agency and the Air Force Research Laboratory.

References

[1] H.C. Liu, F. Capasso (Eds.), Intersubband Transitions in Quantum Wells: Physics and Device Applications I and II, Academic Press, San Diego, 2000.

[2] S.D. Gunapala, J.K. Liu, J.S. Park, T.L. Lin, M. Sundaram, Infrared Radiation Detecting Device, US Patent No. 6,211,529.

[3] Sarath D. Gunapala, John K. Liu, Jin S. Park, Mani Sundaram, Craig A. Shott, Ted Hoelter, True-Lon Lin, S.T. Massie, Paul D. Maker, Richard E. Muller, Gabby Sarusi, 9 μm cutoff 256×256 $Al_xGa1{-}x$As/$Al_xGa1{-}x$As quantum well infrared photodetector hand-held camera, IEEE Trans. Electron Dev. 44 (1997) 51–57.

[4] Sarath D. Gunapala, Sumith V. Bandara, John K. Liu, Winn Hong, Mani Sundaram, Paul D. Maker, Richard E. Muller, Craig A. Shott, Ronald Carralejo, Long-wavelength 640×486 GaAs/$Al_xGa1{-}x$As quantum well infrared photodetector snap-shot camera, IEEE Trans. Electron Dev. 45 (1998) 1890.

[5] W. Cabanski, R. Breiter, R. Koch, K.H. Mauk, W. Rode, J. Ziegler, H. Schneider, M. Walther, R. Oelmaier, 3rd gen focal plane array IR detection modules at AIM, SPIE 4369 (2001) 547–558.

[6] S.D. Gunapala, S.V. Bandara, Quantum well infrared photodetector (QWIP) focal plane arrays, Semiconductors and Semimetals, vol. 62, Academic Press, 1999, pp. 197–282.

[7] S.D. Gunapala, S.V. Bandara, A. Singh, J.K. Liu, S.B. Rafol, E.M. Luong, J.M. Mumolo, N.Q. Tran, J.D. Vincent, C.A. Shott, J. Long, P.D. LeVan, 640×486 long-wavelength two-color GaAs/AlGaAs quantum well infrared photodetector (QWIP) focal plane array camera, IEEE Trans. Electron Dev. 47 (2000) 963–971.

[8] S.D. Gunapala, S.V. Bandara, J.K. Liu, E.M. Luong, N. Stetson, C.A. Shott, J.J. Bock, S.B. Rafol, J.M. Mumolo, M.J. McKelvey, Long-wavelength 256×256 GaAs/AlGaAs quantum well infrared photodetector (QWIP) palm-size camera, IEEE Trans. Electron Dev. 47 (2000) 326–332.

[9] E. Costard, Ph. Bois, X. Marcadet, A. Nedelcu, QWIP products and building blocks for higher performance systems, SPIE 5406 (2004) 646–653.

[10] A. Goldberg, P.N. Uppal, M. Winn, Detection of buried land mines using a dual-band LWIR/LWIR QWIP focal plane array, Infrared Phys. Technol. 44 (2003) 309–324.

[11] H. Schneider, P. Koidl, M. Walther, J. Fleissner, R. Rehm, E. Diwo, K. Schwarz, G. Weimann, Ten years of QWIP development at Fraunhofer IAF, Infrared Phys. Technol. 42 (2001) 283–290.

[12] M.Z. Tidrow, W.R. Dyer, Infrared sensors for ballistic missile defense, Infrared Phys. Technol. 42 (2001) 283–290.

[13] W.A. Beck, Photoconductive gain and generation-recombination noise in multiple-quantum-well infrared detectors, Appl. Phys. Lett. 63 (1993) 3589–3591.

[14] K.K. Choi, C.H. Lin, K.M. Leung, T. Tamir, J. Mao, D.C. Tsui, M. Jhabvala, Broadband and narrow band light coupling for QWIPs, Infrared Phys. Technol. 44 (2003) 309–324.

[15] J.Y. Andersson, L. Lundqvist, Z.F. Paska, Quantum efficiency enhancement of AlGaAs/GaAs quantum well infrared detectors using a waveguide with a grating coupler, Appl. Phys. Lett. 58 (1991) 2264–2267.

[16] S.D. Gunapala, S.V. Bandara, GaAs/AlGaAs multi-quantum well-based infrared focal plane arrays for infrared imaging applications, International Journal of High Speed Electronics and Systems 12 (3) (2002) 99–121.

[17] Sarath D. Gunapala, Sumith V. Bandara, John K. Liu, Sir B. Rafol, Jason M. Mumolo, 640×512 pixel long-wavelength infrared narrowband, multiband, and broadband QWIP focal plane arrays, IEEE Trans. Electron Dev. 50 (2003) 2353–2360.

[18] C.H. Lin, K.M. Leung, T. Tamir, Modal transmission-line theory of three-dimensional periodic structures with arbitrary lattice configurations, J. Opt. Soc. Am. A19 (2002) 2005–2017.

[19] S.D. Gunapala, B.F. Levine, D. Ritter, R. Hamm, M.B. Panish, InGaAs/InP long wavelength quantum well infrared photodetectors, Appl. Phys. Lett. 58 (1991) 2024–2026.

[20] A. Goldberg, T. Fischer, S. Kennerly, S. Wang, M. Sundaram, P. Uppal, M. Winn, G. Milne, M. Stevens, Dualband QWIP MWIR/LWIR focal plane array test results, SPIE 4029 (2000) 276.